ACS APPLIED MATERIALS & INTERFACES

Research Article

www.acsami.org

Platinum Nanoparticle Decorated SiO_2 Microfibers as Catalysts for Micro Unmanned Underwater Vehicle Propulsion

Bolin Chen,[†] Nathaniel T. Garland,[†] Jason Geder,[§] Marius Pruessner,[∥] Eric Mootz,[†] Allison Cargill,[†] Anne Leners,[†] Granit Vokshi,[†] Jacob Davis,[†] Wyatt Burns,[†] Michael A. Daniele,[⊥,#] Josh Kogot,[▽] Igor L. Medintz,[∥] and Jonathan C. Claussen*[,†,‡]

[†]Department of Mechanical Engineering, Iowa State University, Ames, Iowa 50011, United States

[‡]Research Ames Laboratory, Ames, Iowa 50011, United States

[§]Laboratories for Computational Physics and Fluid Dynamics, Code 6041, U.S. Naval Research Laboratory, 4555 Overlook Ave. SW, Washington, DC 20375, United States

[∥]Center for Bio/Molecular Science & Engineering, Code 6900, U.S. Naval Research Laboratory, 4555 Overlook Ave. SW, Washington, DC 20375, United States

[⊥]Department of Electrical and Computer Engineering, North Carolina State University, Raleigh, North Carolina 27606, United States

[#]Joint Department of Biomedical Engineering, University of North Carolina-Chapel Hill/North Carolina State University, Raleigh, North Carolina 27695, United States

[▽]Naval Surface Warfare Center, Panama City, Florida 32407, United States

ABSTRACT: Micro unmanned underwater vehicles (UUVs) need to house propulsion mechanisms that are small in size but sufficiently powerful to deliver on-demand acceleration for tight radius turns, burst-driven docking maneuvers, and low-speed course corrections. Recently, small-scale hydrogen peroxide (H_2O_2) propulsion mechanisms have shown great promise in delivering pulsatile thrust for such acceleration needs. However, the need for robust, high surface area nanocatalysts that can be manufactured on a large scale for integration into micro UUV reaction chambers is still needed. In this report, a thermal/electrical insulator, silicon oxide (SiO_2) microfibers, is used as a support for platinum nanoparticle (PtNP) catalysts. The mercapto-silanization of the SiO_2 microfibers enables strong covalent attachment with PtNPs, and the resultant PtNP−SiO_2 fibers act as a robust, high surface area catalyst for H_2O_2 decomposition. The PtNP−SiO_2 catalysts are fitted inside a micro UUV reaction chamber for vehicular propulsion; the catalysts can propel a micro UUV for 5.9 m at a velocity of 1.18 m/s with 50 mL of 50% (w/w) H_2O_2. The concomitance of facile fabrication, economic and scalable processing, and high performance—including a reduction in H_2O_2 decomposition activation energy of 40−50% over conventional material catalysts—paves the way for using these nanostructured microfibers in modern, small-scale underwater vehicle propulsion systems.

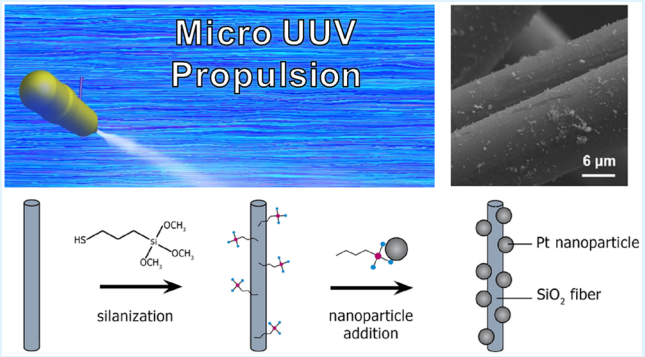

KEYWORDS: *platinum nanoparticles, silicon microfibers, propulsion, hydrogen peroxide, micro unmanned underwater vehicles*

INTRODUCTION

Micro UUVs, or vehicles measuring between half a meter and a few centimeters in length, are advantageous for a variety of applications including characterization of 3D flow dynamics,[1] remote oceanic environmental monitoring,[2] and ocean floor surveying and reconnaissance;[3] all of which shed new light on our understanding of marine life. Moreover, such remote exploration is not limited to littoral waters but may soon include a wide variety of under ice exploration such as exploration of Saturn's moon Europa,[4] which are becoming more approachable with new technologies. These underwater missions require vehicles with the ability to perform tight radius turns, burst-driven docking maneuvers, and low-speed course corrections.[5] In order to provide the micro UUVs with these capabilities, jet propulsion technologies are beginning to replace propeller-based systems which are more prevalent on larger unmanned underwater vehicles. This jet propulsion can be accomplished using energy dense fuel systems such as bipropellant rockets,[6] air-breathing engines, supercapacitors, thermal batteries, and Ni−Cd or Ag−Zn batteries.[7] However, monopropellant and cold gas thrusters greatly outperform said propulsion systems, showing up to 45 times the maximum

Received: August 15, 2016
Accepted: October 11, 2016
Published: October 11, 2016

DOI: 10.1021/acsami.6b10047
ACS Appl. Mater. Interfaces 2016, 8, 30941−30947

power density of Ni−Cd batteries in small-scale applications.[7] In particular, the monopropellant H_2O_2 shows promise for propulsion and has already been used by NASA in reaction control systems, primarily to generate thrust for 100 kg satellites.[8]

H_2O_2 can be decomposed catalytically to produce steam and oxygen at high temperatures, making it an environmentally friendly fuel.[9] Furthermore, H_2O_2 has a large power density with a high specific thrust when compared to other green monopropellants.[10] Many different catalysts have been utilized to initiate H_2O_2 decomposition for both macroscale and micro/nanoscale applications including self-propelled microbots,[11−13] and polymer-based nanorockets.[14−16] H_2O_2 decomposition catalysts have been fabricated using a range of materials such as metal oxides[17−19] (e.g., iron(III) oxide, manganese dioxide, and potassium dichromate), metals such as silver (Ag)[14] and platinum (Pt),[9] and bimetals such as Pt−palladium (Pt−Pd).[15] Metal oxides are consumed during H_2O_2 decomposition and, therefore, can negatively impact propulsion and mission duration. Conversely, Pt metal has been shown to produce catalysts with lower activation energy than all other group VIII metals,[20] and nanostructured Pt nanoparticle (Pt-NP) nanowires have shown lower activation energies than Pt−Pd catalysts.[9] This superior performance makes Pt catalysts well-suited for H_2O_2 decomposition as demonstrated in a wide variety of small-scale applications including sensors/biosensors,[21−23] Pt-loaded stomatocytes,[24] tubular bubble thrusters or nanomotors/microengines,[25] and microelectromechanical system (MEMS) based thrusters.[26]

PtNPs have been grown on a wide variety of substrates including highly conductive surfaces such as graphene,[27−29] carbon nanotubes (CNTs),[30,31] and graphene foam,[32] as well as nonconductive surfaces such as oxides (e.g., SiO_2, aluminum oxide),[33] and paper/cellulose.[34] Templates such as mesoporous silica networks, polycarbonate, and porous anodic alumina are often employed to form Pt nanoparticles/nanowires onto surfaces via electrodeposition.[35,36] Decoration of PtNPs onto surfaces via nontemplated growth methods has also been developed, along with PtNP surface immobilization via covalent linkage, encapsulation, adsorption, biomolecule−nanoparticle binding, and controlled (e.g., current-pulse) electrodeposition.[37,38] Deposition by the reduction of chloroplatinic acid is a simple, one-step process offering several advantages. Most notably, the morphology and density of PtNPs on carbon structures can be controlled by varying the Pt salt bath concentration, pH, and deposition time.[39] In our previous work, we have also shown electroless deposition of Pt nanowires on carbon nanotube microchannel membranes[40] grown through chemical vapor deposition as well as on microfiberous cellulose films.[9,40] However, this work uniquely applies these techniques to a non-carbon, thermal insulator substrate (i.e., SiO_2—one of the most abundant materials on earth) to produce an inexpensive, robust, and efficient catalyst for micro UUV propulsion.

Herein, we apply an electroless, template-free Pt deposition technique to produce PtNPs on nonconductive SiO_2 microfibers via the reduction of chloroplatinic acid (H_2PtCl_6) by formic acid (HCOOH). Pt is nucleated on the SiO_2 microfibers and subsequently forms an even coating of "spherical-like" nanoparticles on the microfiber surface. This spherical nanoparticle morphology is distinct from the Pt nanowire "urchin-like" structures that we previously developed using similar techniques on carbon-based structures including cellulose and carbon nanotubes (CNTs).[9,40] We demonstrate that catalytic conversion of H_2O_2 to oxygen and water provided by the Pt−SiO_2 microfibers provides sufficient thrust to propel micro UUVs while only adding a few grams of weight to the vehicle. Thus, this novel nanostructured catalyst provides a robust, low weight solution for the pulsatile propulsion of micro UUVs—an emerging field of research[9,40,41] nestled between, in terms of length scale, recent advances in H_2O_2 nano/microscale motors[5,11−16,22,42−44] and large-scale satellites.[45,46]

MATERIALS AND METHODS

Mercaptosilane Modification of SiO_2 Microfibers. Before silanization, SiO_2 microfibers (Sigma-Aldrich) were washed by ultrasonication in deionized water (18 MΩ·cm) for 30 min and soaked in 1 M NaOH for 30 min. The mercaptosilane [-(mercaptopropyl)trimethoxysilane, Sigma-Aldrich] was diluted with acetone to 2% (v/v), and the SiO_2 microfibers were incubated in the solution for 3 h at room temperature, and then triple rinsed with acetone and dried under vacuum at 65 °C for 60 min (Figure 1a,b).

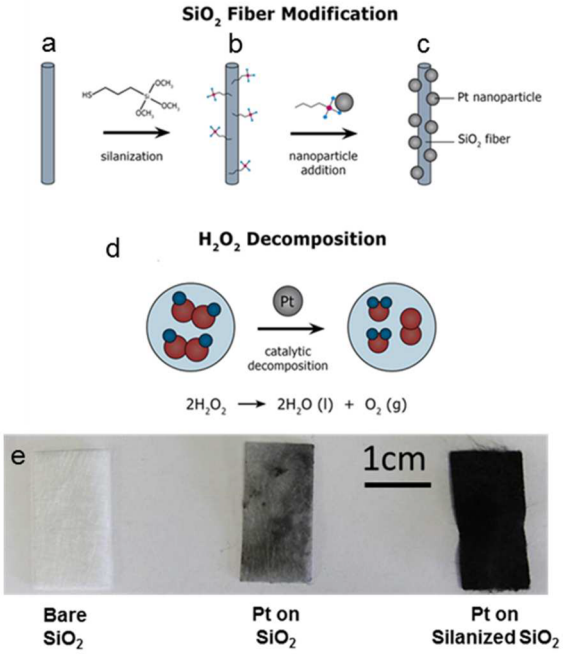

Figure 1. Unmodified silicone oxide fibers (a) are silanized—coated with organofunctional molecules via self-assembly (b)—so that bonds can form which link nanoparticles to the fibers (c). H_2O_2 is decomposed via catalytic decomposition (d), which produces a pressure increase that is monitored to evaluate power produced. (e) Optical image showing size of glass wool microfiber mat (left) and concentration of Pt coated on glass wool fiber mat without silane treatment (middle) and with silane treatment (right).

PtNPs Growth on SiO_2 Microfibers. A solution of chloroplatinic acid hexahydrate, formic acid, and deionized water is used to initiate Pt growth (Figure 1c). Three different solutions were created with varying amounts of chloroplatinic acid hexahydrate (37.5% Pt, Sigma-Aldrich 206083). Each solution contained 2 mL of reagent grade formic acid (88% HCOOH, Macron 2592-05) and 18 mL of deionized water, to which chloroplatinic acid hexahydrate was added—360, 180, and 90 mg in each respective solution, creating three different strength solutions: 34.7, 17.4, and 8.7 mM, respectively. Aliquots of concentrated ammonium hydroxide solution (30.0% NH_3 basis) were added to said metal salt solutions until each mixture had a pH of 1.75. After the solutions were prepared, mercaptosilane-coated glass wool microfibers were placed in each mixture and left to soak for

DOI: 10.1021/acsami.6b10047
ACS Appl. Mater. Interfaces 2016, 8, 30941−30947

approximately 16 h. The glass wool microfibers were finally rinsed thrice with deionized water and air-dried at room temperature.

H_2O_2 Decomposition. H_2O_2 decomposition testing was performed according to our previous protocols[9,40] for each catalyst sample (34.7, 17.4, and 8.7 mM) at three different temperatures (0, 17.5, 35 °C). In brief, a concentration of 1% H_2O_2 (diluted from 30% w/w in H_2O_2 from the manufacturer: Fisher Scientific BP2633-500) was used. The mass of Pt−SiO_2 catalyst used in each test was held constant at 0.03 g to make a more accurate assessment of the effectiveness of each developed catalyst with distinct molar concentrations of Pt salt. The test apparatus included two 125 mL round-bottom glass flasks—one to test the catalyst and the other as a control flask without catalyst. Magnetic stir bars were positioned in the bottom of the flasks to simulate a "flowing" environment, thus maximizing the amount of H_2O_2 contacting the catalyst sample. The flasks are placed inside water baths on top of magnetic stirrer hot plates to maintain quasi isothermal conditions at 17.5 and 35 °C, respectively, while the flasks were placed in ice water baths to maintain the flask temperatures at 0 °C. A thermometer was dipped into the bath solutions to monitor and adjust the bath temperatures accordingly. The amount of oxygen generated during each test was represented as a pressure differential between the testing (PtNP−SiO_2 and H_2O_2 reaction) and reference environments. Pressure differences versus time were graphically displayed on a computer. In between each trial run, the nanowires were removed from the flask with tweezers and dried to ensure a maximum reaction for the following runs. Resultant differential pressure vs time data were then used to determine catalyst efficiency, as shown in the Results and Discussion section.

Micro UUV Fabrication and Testing. The micro UUV was designed in SolidWorks, a computer aided design program, then manufactured with an Objet500 Connex 3D Printer using a PMMA-like resin for the printing material. Once fabricated, the micro UUV was attached to a 30.5 in. (0.77 m) rigid arm via screw thread fastening and submerged in a 350 gal tank filled with 250 gal of water. The opposite end of the arm was attached to a torque transducer (Interface model 5350-50:50 oz-in sensor) mounted above the water tank. The transducer was capable of measuring torque moments about the neutral axis of the micro UUV within a 0.001 N·m tolerance, and the readings were outputted via a CPU connection. The thrust produced by the micro UUV was calculated from the torque readings using software on the CPU. High-purity H_2O_2 was pumped into the reaction chamber with a 50 mL syringe through a high strength silicone tube (inner dia. 0.25 in./9.525 mm) fitted to the reaction chamber via a plastic barbed fitting. Steady flow rates were produced by applying a constant pressure via a syringe pump connected to the syringe. Pulsating flow was produced by manually applying pressure to the syringe. Note this micro UUV was designed to rigidly attach to the strain gauge to measured underwater vehicle thrust measurements via the decomposition of H_2O_2 with the developed Pt−SiO_2 catalyst; the developed micro UUV was not designed for free swimming.

RESULTS AND DISCUSSION

Design and Fabrication of Pt−SiO_2. In previous studies, mercaptosilane-activated surfaces have permitted direct coupling of oligonucleotides to glass surfaces[37] and enzymes to platinized surfaces.[9] Such glass-silanization and Pt-silanization techniques offer strong lateral stabilization of biological agents through covalent linkages. These techniques form the chemical modification rationale for this work, in that we hypothesize that mercaptosilane-activated SiO_2 fibers will form strong covalent linkages with PtNPs. Figure 1a−c shows a schematic of these silanization processes. A low pH (1.75) was selected to create the needle-like Pt nanowires, as our previously published work demonstrated that this low pH assists in the development of dense PtNPs onto surfaces, namely, cellulose and CNTs.[9,40] Figure 1e qualitatively illustrates how mercaptosilane-activated SiO_2 promotes the deposition of PtNPs onto the SiO_2 fibers, where Pt nanoparticle density (black) is much denser on mercaptosilane-activated SiO_2 fibers as compared to those that are not. Scanning electron microscopy (SEM) micrographs of these Pt dense SiO_2 fibers reveal a surface coverage of PtNPs with large micro/macro cloudlike PtNPs at higher chloroplatinic acid hexahydrate concentrations, i.e., 34.7 mM (Figure 2). The size and density of these Pt structures are subsequently improved for enhanced catalytic decomposition of H_2O_2.

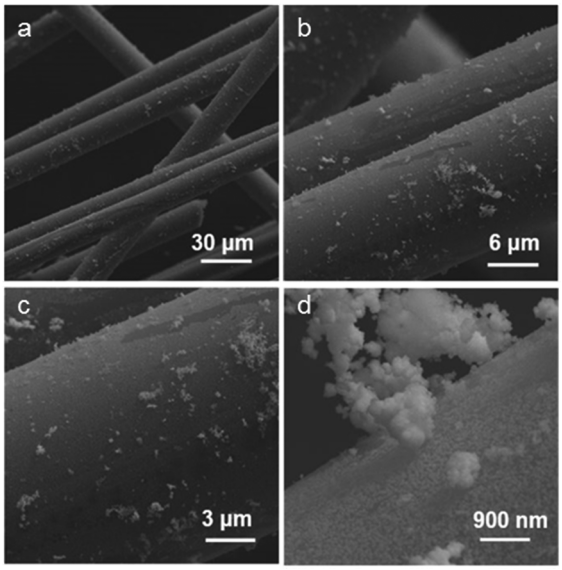

Figure 2. Scanning electron microscopy (SEM) images obtained at 20 keV show the size, density, and morphology of Pt nanoparticles and macro/microparticles decorated on mercaptosilane-activated SiO_2 microfibers with 34.7 mM chloroplatinic acid hexahydrate. The SEM magnification is (a) 1 k×, (b) 5 k×, (c) 10 k× and (d) 40 k×, respectively.

The size and density of the PtNPs can be tuned by adjusting the concentration of the Pt salt bath used in the deposition process. For example, a 34.7 mM chloroplatinic acid hexahydrate concentration produces highly aggregated nanoparticles with larger micro/macroparticles on the mercaptosilane-activated SiO_2 (Figure 3a). The density of the PtNPs significantly decreases while the relative number of larger micro/macroparticles stays relatively the same when the chloroplatinic acid hexahydrate concentration is reduced by half to 17.4 mM (Figure 3b). Finally, a monodisperse layer of PtNPs without larger micro/macroparticles is formed on the mercaptosilane-activated SiO_2 by reducing the chloroplatinic acid hexahydrate concentration by half again to 8.7 mM (Figure 3c). The effects of this dense, uniform surface coverage of PtNPs on the SiO_2 microfiber surface significantly improves the reaction kinetics of the decomposition of H_2O_2 as compared to the other Pt−SiO_2 microfibers (Figure 3d). These reaction kinetics are discussed in detail in the next section of the paper.

Catalyst Characterization: H_2O_2 Decomposition. It is known that the effectiveness of Pt catalysts for H_2O_2 decomposition is proportional to the contact area between Pt and H_2O_2, as higher exposed surface area leads to increased likelihood for Pt-(-OH) and Pt-(-H) binding.[19] The reaction of H_2O_2 decomposition at low temperatures produces liquid water and oxygen (eq 1).

$$2H_2O_2 \rightarrow 2H_2O(l) + O_2(g) \quad (1)$$

DOI: 10.1021/acsami.6b10047
ACS Appl. Mater. Interfaces 2016, 8, 30941−30947

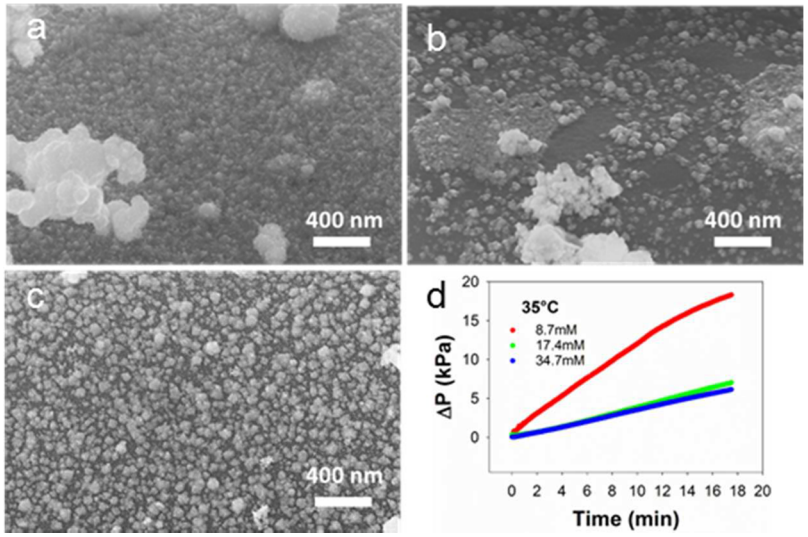

Figure 3. Scanning electron microscopy (SEM) images (magnification of 100 k×) obtained at 20 keV show the difference of size, density, and distribution of Pt particles deposited on the mercaptosilane-activated SiO_2 microfibers with distinct chloroplatinic acid hexahydrate concentrations of (a) 34.7, (b) 17.4, and (c) 8.7 mM. Measured differential pressure vs time data (d) taken as the average of three test runs per sample at 35 °C for Pt−SiO_2 with 8.7 mM (red), 17.4 mM (green), and 34.7 mM (blue) chloroplatinic acid hexahydrate concentrations.

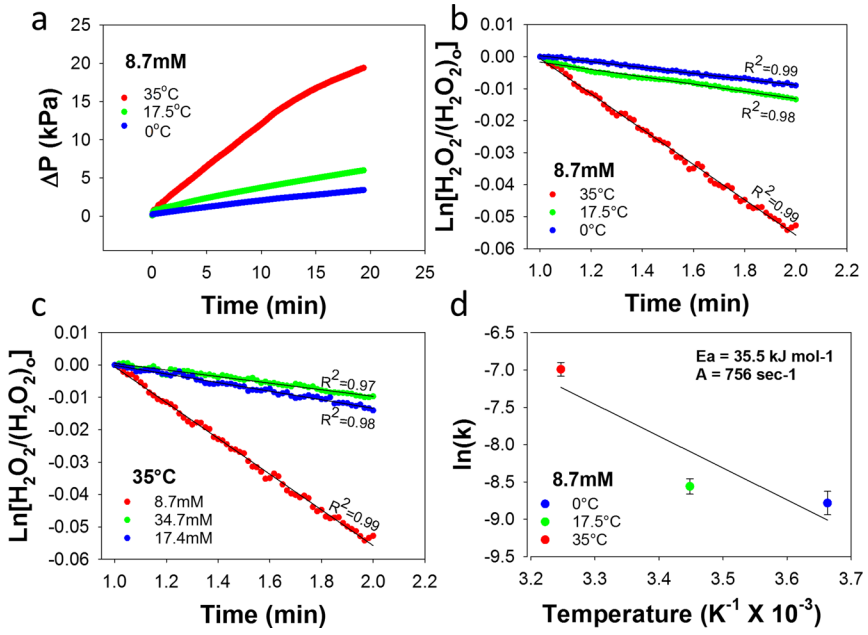

Figure 4. (a) Reaction rate plots calculated according to eq 3, using the data from Figure 3d. (b) Measured differential pressure vs time data taken as the average of three test runs for Pt−SiO_2 catalyst (8.7 mM), performed at three temperatures: 0, 1.75, and 35 °C. (c) Reaction rate plots calculated using eq 3 and data from plot (b). (d) Plot of the natural log of the Arrhenius equation for Pt−SiO_2 catalyst (8.7 mM) immersed in 1% w/w H_2O_2 solution at three distinct temperatures (0, 17, and 35 °C); slope used to determine activation energy. Errors bars represent one standard deviation from the mean (n = 3).

The oxygen generated by 1% H_2O_2 decomposition from each of the developed catalysts formed with distinct Pt salt concentrations viz., 34.7, 17.4, and 8.7 mM, was monitored via generated pressure in order to ascertain the effectiveness of each catalyst (see Results and Discussion, Figure 3d). The Pt−SiO_2 microfibers fabricated with 8.7 mM chloroplatinic acid hexahydrate concentration displayed the largest total amount of generated pressure (i.e., oxygen) as well as the most rapid reaction rate over the 18 min experiment obtained at a controlled temperature of 35 °C (Figure 3d). The ideal gas law ($PV = nRT$) is subsequently used to calculate the moles of oxygen (n) generated during the reaction, where P is the measured differential pressure (kPa), V is the volume of the flask (125 mL), R is the ideal gas constant (8.314 J mol^{-1} K^{-1}), and T is the bath temperature (K). Next, the apparent kinetic constant (k_{obs}) is determined by the slope of the natural logarithm of the concentration of hydrogen peroxide versus time displayed in Figure 4a and acquired from eq 2

$$\ln \frac{[H_2O_2]}{[H_2O_2]_0} = k_{obs}t \tag{2}$$

where $[H_2O_2]$ is the amount of H_2O_2 remaining in solution at time t and $[H_2O_2]_0$ is the initial amount of H_2O_2 in the

DOI: 10.1021/acsami.6b10047
ACS Appl. Mater. Interfaces 2016, 8, 30941−30947

solution. The decomposition of H_2O_2 followed first-order reaction kinetics (eq 2) as verified in the high degree of linearity in the reaction rate plot (Figure 4a). These first-order reaction kinetics followed similar reports that have analyzed decomposition of H_2O_2 with Pt, Pt−Pd, Fe, MnO_2, $K_2Cr_2O_7$, and Au.[47−50] The calculated k_{obs} values for the Pt−SiO_2 catalyst (8.7 mM) at 35, 17.5, and 0 °C were calculated from the slope of Figure 4c to be 0.694 ± 0.106, 0.250 ± 0.185, and 0.116 ± 0.128, respectively, where error is ± one standard deviation and n = 3. These Pt−SiO_2 catalyst (8.7 mM) k_{obs} values are related to the activation energy (E_a) through the Arrhenius equation (eq 3).

$$k_{obs} = Ae^{-E_a/RT} \tag{3}$$

The E_a can be acquired by plotting the natural logarithm of the k_{obs} vs the inverse of temperature (see eq 4 and the Arrhenius plot in Figure 4d).

$$\ln(k_{obs}) = \frac{-E_a}{R}\frac{1}{T} + \ln(A) \tag{4}$$

The E_a of the Pt−SiO_2 catalyst (8.7 mM) is acquired (35.5 kJ/mol) from the slope of the Arrhenius plot ($-E_a/R$) (see Table 1). Table 1 shows the reaction rate constants and activation energy calculated from the pressure data. The large standard deviation in k_{obs} for this catalyst can likely be attributed to quality control and damage inflicted on the catalyst during extraction from the pressure chamber. While the activation energy is higher than that of our reported Pt-CNT-membrane (E_a = 24.0 kJ mol^{-1}), it is still comparable to Pt/palladium nanoparticles on Nafion (E_a = 34.0−36.3 kJ mol^{-1})[47] and is able to lower the activation energy by 40−55% over conventional materials (ferrihydrates, iron oxide, and pyrite) used in H_2O_2 decomposition.[8,33]

Table 1. H_2O_2 Decomposition Kinetics for Pt−SiO_2

T (K)	k_{obs} ($s^{-1} \times 10^{-3}$)	E_a (kJ mol^{-1})	A (s^{-1})	ΔS (J mol^{-1} K^{-1})
273	−0.116 ± 0.128			
291	−0.250 ± 0.185	35.5	689.3	54.3
308	−0.694 ± 0.106			

Micro UUV Propulsion. A micro UUV prototype was fabricated in order to test the thrust generated by the H_2O_2 decomposition (Figure 5b,c). Eight Pt−SiO_2 samples, created with a Pt salt concentration of 8.7 mM and a subsequent surface area of 2.87 cm^2 (Figure 5d), were loaded into the test micro UUV. The micro UUV was designed to rigidly attach to the strain gauge (i.e., not designed for free swimming), and therefore, drag characteristics were not considered in said design. However, the micro UUV was designed with a convergent exit nozzle, limiting the exit flow to sonic or subsonic speeds. The micro UUV reaction chamber and exit nozzle were constructed with a volume of 1.2 × 10^{-5} m^3 and cross-sectional area of 1.8 × 10^{-5} m^2, respectively, to provide sufficient thrust for experimental monitoring as developed in our previous protocols.[9,40] The thrust generated was measured by a strain gauge that was mounted to the micro UUV. Syringe-fed tubing was secured to the inlet of the micro UUV for injecting H_2O_2 into the micro UUV chamber. Then, the micro UUV was placed into a water tank for testing (Figure 5a and Materials and Methods section). The eight Pt−SiO_2 samples embedded in the micro UUV reaction chamber generated a thrust of 26 mN ± 0.498 (±1 std, n = 3) over 5 s (flow rate ∼ 10 mL s^{-1}) for a H_2O_2 fuel concentration of 50% w/w. These thrust measurements are comparable to the thrust achieved with 30% w/w H_2O_2 fuel with a similar flow rate with our previous Pt-cellulose[9,40] and Pt-CNT-membranes[40] catalysts. Furthermore, control experiments show that water injected at the maximum flow rates tested herein produce negligible thrust (data not shown); therefore, all measured thrust is attributed to the decomposition of hydrogen peroxide by the Pt−SiO_2 catalyst. The reported thrust values for each combination of test conditions were taken from the average of three runs per condition (Figure 5e). The calculated average velocity for the micro UUV is 1.2 m s^{-1}, by using the following steady-state thrust/drag equation

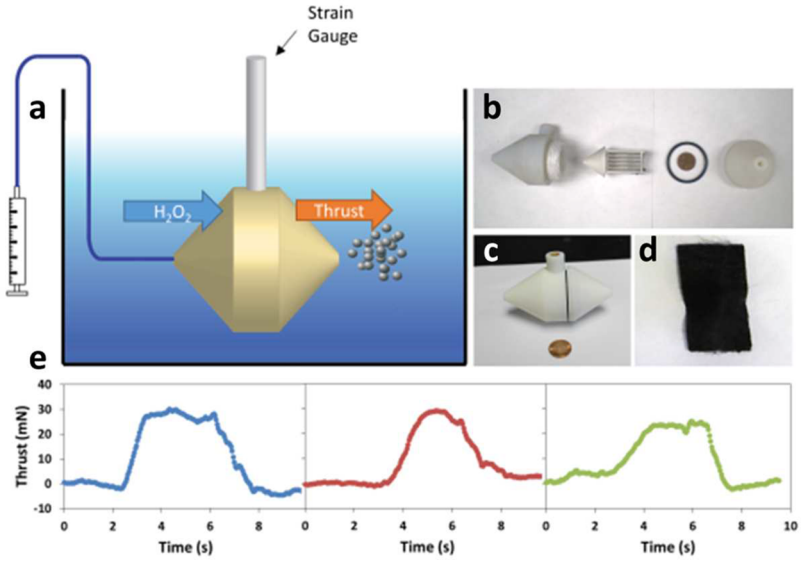

Figure 5. (a) Schematic illustrating water tank setup and strain gauge used to monitor thrust. (b) Optical image showing disassembled test parts and size. (c) Optical image showing assembled test parts and size (d) 2 cm^2 Pt−SiO_2 sample loaded in the reaction chamber. (e) Generated thrust from H_2O_2 (50 mL of 50% w/w) injected into the reaction chamber with Pt−SiO_2 catalyst developed with 8.7 mM Pt salt concentration.

DOI: 10.1021/acsami.6b10047
ACS Appl. Mater. Interfaces 2016, 8, 30941−30947

$$v = \sqrt{\frac{2T}{C_D \rho A}} \quad (5)$$

where T (26.9 mN) is the thrust generated by H_2O_2 decomposition with drag coefficient (C_D) equal to 0.04 and a cylindrical body with a diameter-to-length ratio of 1:6, ρ is the density of surrounding fluid (H_2O), and A is the cross-sectional area of the micro UUV (9.7 cm^2). Specific impulse (28.9 m s^{-1}) is calculated by using

$$I_{sp} = \frac{T}{\dot{m}} \quad (6)$$

where T is thrust and ($\dot{m}$) is the mass flow rate, which is 0.93 g s^{-1} (50 mL min^{-1}). Hence, the PtNP−SiO_2 catalysts can propel a micro UUV for 5.9 m at a velocity of 1.18 m/s for 5 s with 50 mL of 50% (w/w) H_2O_2.

CONCLUSIONS

This work demonstrates how PtNPs can be deposited onto mercaptosilane-modified SiO_2 via a facile chemical reduction method. The spherical-like PtNPs can be uniformly deposited in a monodisperse fashion onto the entirety of the SiO_2 by modifying the concentration of the Pt in the electrodeposition salt solution. Pt−SiO_2 catalyst characterization demonstrated the potential capability of moving a small underwater vehicle 6 m in just under 6 s with just 50 mL of H_2O_2 fuel. The average thrust obtained (26 mN ± 0.498) in this work meets the millinewton thrust requirements for attitude adjustment with micro/nanosatellites and micro UUV propulsion for forward movement, hovering/loitering, or docking maneuvers.[51,52]

Recent research has shown that nanostructured Pt is well-suited for H_2O_2 decomposition for nano/microscale propulsion. For example, nano/microscale Pt has been able to assist in propelling motion-controllable nanoscale vehicles[53] that can be propelled in a wide range of liquids including within oil contaminants.[42] PtNPs have also been used in stomatocytes for use in the body[24] and in drug delivery.[54] For larger-scale applications, H_2O_2 has been used to propel satellites,[8] larger rockets[6] by NASA, and even World War 1-era torpedoes with rocket-grade H_2O_2.[45,46] In this work, our advancements are in propelling small hand-held size vehicles or micro UUVs with nanostructured catalysts for highly efficient propulsion of small vehicles, which demonstrates that nanotechnology can be incorporated into small hand-held applications. This work also demonstrates that these nanostructured catalysts could be used in small underwater vehicles, but also potentially in small satellites or rockets. Future work includes optimizing the shape of the exit nozzle to also maximize micro UUV thrust.

AUTHOR INFORMATION

Corresponding Author

*E-mail: jcclauss@iastate.edu.

Notes

The authors declare no competing financial interest.

ACKNOWLEDGMENTS

The authors gratefully acknowledge funding assistance from the Naval Surface Warfare Center (NSWC) in Panama City (award #N61331-16-P-4551), the Naval Research Laboratory in Washington, DC, as well as from the Department of Mechanical Engineering and College of Engineering at Iowa State University.

REFERENCES

(1) Hobson, B.; Schulz, B.; Janet, J.; Kemp, M.; Moody, R.; Pell, C.; Pinnix, H. Development of a Micro Autonomous Underwater Vehicle for Complex 3-D Sensing. In *OCEANS, 2001. MTS/IEEE Conference and Exhibition*; 2001; Vol. *4*, pp 2043−2045.

(2) Desa, E.; Madhan, R.; Maurya, P. Potential of Autonomous Underwater Vehicles as New Generation Ocean Data Platforms. *Curr. Sci.* **2006**, *90*, 1202−1209.

(3) Bishop, G. C. Gravitational Field Maps and Navigational Errors [Unmanned Underwater Vehicles]. *IEEE J. Oceanic Eng.* **2002**, *27*, 726−737.

(4) Bowen, A.; Jakuba, M.; Yoerger, D.; German, C.; Kinsey, J. C.; Whitcomb, L. L.; Mayer, L. Lightly Tethered Unmanned Underwater Vehicle for Under-Ice Exploration. In *Aerospace Conference, 2012 IEEE*, March 3−10, 2012; IEEE: Piscataway, NJ, 2012; pp 1−12.

(5) Nawroth, J. C.; Lee, H.; Feinberg, A. W.; Ripplinger, C. M.; McCain, M. L.; Grosberg, A.; Dabiri, J. O.; Parker, K. K. A Tissue-Engineered Jellyfish with Biomimetic Propulsion. *Nat. Biotechnol.* **2012**, *30*, 792−797.

(6) Sisco, J. C.; Austin, B.; Mok, J.; Anderson, W. Autoignition of Kerosene by Decomposed Hydrogen Peroxide in a Dump-Combustor Configuration. *J. Propul. Power* **2005**, *21*, 450−459.

(7) Wernimont, E. J. Monopropellant Hydrogen Peroxide Rocket Systems: Optimum for Small Scale. In *42nd AIAA Joint Propulsion Conference and Exhibit*, Sacramento, CA, 2006; AIAA-2006-5235.

(8) Biggs, D.; Conley, J.; Perez, A. D., Faber, N.; Genova, A.; Gonzales, A.; *Small Spacecraft Technology State of the Art* ; NASA STI Program STI Support Services; NASA Langley Research Center: Hampton, VA, 2013.

(9) Claussen, J. C.; Daniele, M. A.; Geder, J.; Pruessner, M.; Mäkinen, A. J.; Melde, B. J.; Twigg, M.; Verbarg, J. M.; Medintz, I. L. Platinum-Paper Micromotors: An Urchin-like Nanohybrid Catalyst for Green Monopropellant Bubble-Thrusters. *ACS Appl. Mater. Interfaces* **2014**, *6*, 17837−17847.

(10) Cheung, W.; Tilston, J. *Hydrogen Peroxide Based Propulsion System for Micro Air Vehicle Applications*; DTIC Document; American Institute of Aeronautics and Astronautics, Inc.: Reston, VA, 1999.

(11) Kumar, S.; Singh, A. K.; Dasmahapatra, A. K.; Mandal, T. K.; Bandyopadhyay, D. Graphene Based Multifunctional Superbots. *Carbon* **2015**, *89*, 31−40.

(12) Singh, A. K.; Dey, K. K.; Chattopadhyay, A.; Mandal, T. K.; Bandyopadhyay, D. Multimodal Chemo-Magnetic Control of Self-Propelling Microbots. *Nanoscale* **2014**, *6*, 1398−1405.

(13) Dey, K. K.; Bhandari, S.; Bandyopadhyay, D.; Basu, S.; Chattopadhyay, A. The pH Taxis of an Intelligent Catalytic Microbot. *Small* **2013**, *9*, 1916−1920.

(14) Wu, Z.; Lin, X.; Wu, Y.; Si, T.; Sun, J.; He, Q. Near-Infrared Light-Triggered "On/Off" Motion of Polymer Multilayer Rockets. *ACS Nano* **2014**, *8*, 6097−6105.

(15) Wu, Z.; Lin, X.; Si, T.; He, Q. Recent Progress on Bioinspired Self-Propelled Micro/Nanomotors via Controlled Molecular Self-Assembly. *Small* **2016**, *12*, 3080−3093.

(16) Wu, Z.; Wu, Y.; He, W.; Lin, X.; Sun, J.; He, Q. Self-Propelled Polymer-Based Multilayer Nanorockets for Transportation and Drug Release. *Angew. Chem., Int. Ed.* **2013**, *52*, 7000−7003.

(17) Huang, H.-H.; Lu, M.-C.; Chen, J.-N. Catalytic Decomposition of Hydrogen Peroxide and 2-chlorophenol with Iron Oxides. *Water Res.* **2001**, *35*, 2291−2299.

(18) Seol, Y.; Javandel, I. Citric Acid-Modified Fenton's Reaction for the Oxidation of Chlorinated Ethylenes in Soil Solution Systems. *Chemosphere* **2008**, *72*, 537−542.

(19) Međedović, S.; Locke, B. R. Platinum Catalysed Decomposition of Hydrogen Peroxide in Aqueous-Phase Pulsed Corona Electrical Discharge. *Appl. Catal., B* **2006**, *67*, 149−159.

(20) McKee, D. W. Catalytic Decomposition of Hydrogen Peroxide by Metals and Alloys of the Platinum Group. *J. Catal.* **1969**, *14*, 355−364.

(21) Claussen, J. C.; Kumar, A.; Jaroch, D. B.; Khawaja, M. H.; Hibbard, A. B.; Porterfield, D. M.; Fisher, T. S. Nanostructuring

DOI: 10.1021/acsami.6b10047
ACS Appl. Mater. Interfaces 2016, 8, 30941−30947

Platinum Nanoparticles on Multilayered Graphene Petal Nanosheets for Electrochemical Biosensing. *Adv. Funct. Mater.* **2012**, *22*, 3399−3405.
(22) Wang, J.; Gao, W. Nano/Microscale Motors: Biomedical Opportunities and Challenges. *ACS Nano* **2012**, *6*, 5745−5751.
(23) Yang, M.; Yang, Y.; Liu, Y.; Shen, G.; Yu, R. Platinum Nanoparticles-Doped Sol−Gel/Carbon Nanotubes Composite Electrochemical Sensors and Biosensors. *Biosens. Bioelectron.* **2006**, *21*, 1125−1131.
(24) Wilson, D. A.; Nolte, R. J.; van Hest, J. C. Entrapment of Metal Nanoparticles in Polymer Stomatocytes. *J. Am. Chem. Soc.* **2012**, *134*, 9894−9897.
(25) Manesh, K. M.; Cardona, M.; Yuan, R.; Clark, M.; Kagan, D.; Balasubramanian, S.; Wang, J. Template-Assisted Fabrication of Salt-Independent Catalytic Tubular Microengines. *ACS Nano* **2010**, *4*, 1799−1804.
(26) An, S.; Lim, H.; Kwon, S. Hydrogen Peroxide Thruster Module for Microsatellites with Platinum Supported by Alumina as Catalyst. In *43rd Joint Propulsion Conference and Exhibit*; 2007; pp 8−11.
(27) Qiu, J.-D.; Wang, G.-C.; Liang, R.-P.; Xia, X.-H.; Yu, H.-W. Controllable Deposition of Platinum Nanoparticles on Graphene as an Electrocatalyst for Direct Methanol Fuel Cells. *J. Phys. Chem. C* **2011**, *115*, 15639−15645.
(28) Si, Y.; Samulski, E. T. Exfoliated Graphene Separated by Platinum Nanoparticles. *Chem. Mater.* **2008**, *20*, 6792−6797.
(29) Guo, S.; Wen, D.; Zhai, Y.; Dong, S.; Wang, E. Platinum Nanoparticle Ensemble-on-Graphene Hybrid Nanosheet: One-Pot, Rapid Synthesis, and Used as New Electrode Material for Electrochemical Sensing. *ACS Nano* **2010**, *4*, 3959−3968.
(30) Xue, B.; Chen, P.; Hong, Q.; Lin, J.; Tan, K. L. Growth of Pd, Pt, Ag and Au Nanoparticles on Carbon Nanotubes. *J. Mater. Chem.* **2001**, *11*, 2378−2381.
(31) Claussen, J. C.; Artiles, M. S.; McLamore, E. S.; Mohanty, S.; Shi, J.; Rickus, J. L.; Fisher, T. S.; Porterfield, D. M. Electrochemical Glutamate Biosensing with Nanocube and Nanosphere Augmented Single-Walled Carbon Nanotube Networks: a Comparative Study. *J. Mater. Chem.* **2011**, *21*, 11224−11231.
(32) Sattayasamitsathit, S.; Gu, Y.; Kaufmann, K.; Jia, W.; Xiao, X.; Rodriguez, M.; Minteer, S.; Cha, J.; Burckel, D. B.; Wang, C.; Polsky, R.; Wang, J. Highly Ordered Multilayered 3D Graphene Decorated with Metal Nanoparticles. *J. Mater. Chem. A* **2013**, *1*, 1639−1645.
(33) Joo, S. H.; Park, J. Y.; Tsung, C.-K.; Yamada, Y.; Yang, P.; Somorjai, G. A. Thermally Stable Pt/Mesoporous Silica Core-Shell Nanocatalysts for High-Temperature Reactions. *Nat. Mater.* **2009**, *8*, 126−131.
(34) Cai, J.; Kimura, S.; Wada, M.; Kuga, S. Nanoporous Cellulose as Metal Nanoparticles Support. *Biomacromolecules* **2009**, *10*, 87−94.
(35) Wang, H.; Jeong, H. Y.; Imura, M.; Wang, L.; Radhakrishnan, L.; Fujita, N.; Castle, T.; Terasaki, O.; Yamauchi, Y. Shape- and Size-Controlled Synthesis in Hard Templates: Sophisticated Chemical Reduction for Mesoporous Monocrystalline Platinum Nanoparticles. *J. Am. Chem. Soc.* **2011**, *133*, 14526−14529.
(36) Wang, H.; Imura, M.; Nemoto, Y.; Park, S. E.; Yamauchi, Y. Synthesis of Olive-Shaped Mesoporous Platinum Nanoparticles (MPNs) with a Hard-Templating Method Using Mesoporous Silica (SBA-15). *Chem. - Asian J.* **2012**, *7*, 802−809.
(37) Ye, H.; Scott, R. W. J.; Crooks, R. M. Synthesis, Characterization, and Surface Immobilization of Platinum and Palladium Nanoparticles Encapsulated within Amine-Terminated Poly(amidoamine) Dendrimers. *Langmuir* **2004**, *20*, 2915−2920.
(38) Katz, E.; Willner, I. Integrated Nanoparticle−Biomolecule Hybrid Systems: Synthesis, Properties, and Applications. *Angew. Chem., Int. Ed.* **2004**, *43*, 6042−6108.
(39) Wang, C.; Daimon, H.; Onodera, T.; Koda, T.; Sun, S. A General Approach to the Size- and Shape-Controlled Synthesis of Platinum Nanoparticles and Their Catalytic Reduction of Oxygen. *Angew. Chem., Int. Ed.* **2008**, *47*, 3588−3591.
(40) Marr, K. M.; Chen, B.; Mootz, E. J.; Geder, J.; Pruessner, M.; Melde, B. J.; Vanfleet, R. R.; Medintz, I. L.; Iverson, B. D.; Claussen, J. C. High Aspect Ratio, Carbon Nanotube Membranes Decorated with Pt Nanoparticle Urchins for Micro Underwater Vehicle Propulsion via H2O2 Decomposition. *ACS Nano* **2015**, *9*, 7791−7803.
(41) Athanassiadis, A. G. Parallel Pulsed Jets for Precise Underwater Propulsion. Thesis, Massachusetts Institute of Technology, Cambridge, MA, 2016.
(42) Baraban, L.; Makarov, D.; Streubel, R.; Mönch, I.; Grimm, D.; Sanchez, S.; Schmidt, O. G. Catalytic Janus Motors on Microfluidic Chip: Deterministic Motion for Targeted Cargo Delivery. *ACS Nano* **2012**, *6*, 3383−3389.
(43) Campuzano, S.; Orozco, J.; Kagan, D.; Guix, M.; Gao, W.; Sattayasamitsathit, S.; Claussen, J. C.; Merkoçi, A.; Wang, J. Bacterial Isolation by Lectin-Modified Microengines. *Nano Lett.* **2012**, *12*, 396−401.
(44) Paxton, W. F.; Kistler, K. C.; Olmeda, C. C.; Sen, A.; St. Angelo, S. K.; Cao, Y.; Mallouk, T. E.; Lammert, P. E.; Crespi, V. H. Catalytic Nanomotors: Autonomous Movement of Striped Nanorods. *J. Am. Chem. Soc.* **2004**, *126*, 13424−13431.
(45) Wernimont, E.; Ventura, M.; Garboden, G.; Mullens, P. *Past and Present Uses of Rocket Grade Hydrogen Peroxide*; 2nd International Hydrogen Peroxide Propulsion Conference, Purdue University, 1999.
(46) Rusek, J. J. New Decomposition Catalysts and Characterization Techniques for Rocket-Grade Hydrogen Peroxide. *J. Propul. Power* **1996**, *12*, 574−579.
(47) Hasnat, M.; Rahman, M. M.; Borhanuddin, S.; Siddiqua, A.; Bahadur, N.; Karim, M. Efficient Hydrogen Peroxide Decomposition on Bimetallic Pt−Pd Surfaces. *Catal. Commun.* **2010**, *12*, 286−291.
(48) Miller, C. M.; Valentine, R. L. Oxidation Behavior of Aqueous Contaminants in the Presence of Hydrogen Peroxide and Filter Media. *J. Hazard. Mater.* **1995**, *41*, 105−116.
(49) Teshima, N.; Genfa, Z.; Dasgupta, P. K. Catalytic Decomposition of Hydrogen Peroxide by a Flow-Through Self-Regulating Platinum Black Heater. *Anal. Chim. Acta* **2004**, *510*, 9−13.
(50) De Laat, J.; Gallard, H. Catalytic Decomposition of Hydrogen Peroxide by Fe (III) in Homogeneous Aqueous Solution: Mechanism and Kinetic Modeling. *Environ. Sci. Technol.* **1999**, *33*, 2726−2732.
(51) De Groot, W. Propulsion Options for Primary Thrust and Attitude Control of Microspacecraft. In *COSPAR Colloquia Series*; Fei-Bin, H., Ed.; Pergamon Press: Oxford, U.K., 1999; Vol. *10*, pp 200−209.
(52) Abershitz, A.; Penn, D.; Levy, A.; Shapira, A.; Shavit, Z.; Tsach, S. IAI's Micro/Mini UAV Systems-Development Approach. In *Infotech@Aerospace Conference*, Arlington, VA, Sept 26−29, 2005; AIAA: Reston, VA, 2005
(53) Wang, J.; Manesh, K. M. Motion Control at the Nanoscale. *Small* **2010**, *6*, 338−345.
(54) Gao, W.; Wang, J. Synthetic Micro/Nanomotors in Drug Delivery. *Nanoscale* **2014**, *6*, 10486−10494.

DOI: 10.1021/acsami.6b10047
ACS Appl. Mater. Interfaces 2016, 8, 30941−30947